Available online at www.sciencedirect.com
ScienceDirect
Medical Engineering & Physics 30 (2008) 9–19
Medical Engineering & Physics
www.elsevier.com/locate/medengphy

Non-Newtonian models for molecular viscosity and wall shear stress in a 3D reconstructed human left coronary artery

Johannes V. Soulis [a], George D. Giannoglou [b,*], Yiannis S. Chatzizisis [b], Kypriani V. Seralidou [a], George E. Parcharidis [b], George E. Louridas [b]

[a] *Fluid Mechanics, Demokrition University of Thrace, Xanthi, Greece*
[b] *Cardiovascular Engineering and Atherosclerosis Laboratory, 1st Cardiology Department, AHEPA University Hospital, Aristotle University of Thessaloniki, 1 St. Kyriakidi Street, 54636 Thessaloniki, Greece*

Received 10 July 2006; received in revised form 26 January 2007; accepted 4 February 2007

Abstract

The capabilities and limitations of various molecular viscosity models, in the left coronary arterial tree, were analyzed via: molecular viscosity, local and global non-Newtonian importance factors, wall shear stress (WSS) and wall shear stress gradient (WSSG). The vessel geometry was acquired using geometrically correct 3D intravascular ultrasound (3D IVUS). Seven non-Newtonian molecular viscosity models, plus the Newtonian one, were compared. The WSS distribution yielded a consistent LCA pattern for nearly all non-Newtonian models. High molecular viscosity, low WSS and low WSSG values occured at the outer walls of the major bifurcation in proximal LCA regions. The Newtonian blood flow was found to be a good approximation at mid- and high-strain rates. The non-Newtonian Power Law, Generalized Power Law, Carreau and Casson and Modified Cross blood viscosity models gave comparable molecular viscosity, WSS and WSSG values. The Power Law and Walburn–Schneck models over-estimated the non-Newtonian global importance factor I_G and under-estimated the area averaged WSS and WSSG values. The non-Newtonian Power Law and the Generalized Power Law blood viscosity models were found to approximate the molecular viscosity and WSS calculations in a more satisfactory way.

Keywords: Non-Newtonian blood flow; Wall shear stress; Coronary artery; Intravascular ultrasound

1. Background

The hemodynamic conditions of the cardiovascular system are highly influenced by molecular viscosity of the blood, the velocity strain rate, the static pressure and the wall shear stress (WSS). The role of viscosity in the development and progression of coronary atherosclerosis is important [1,2]. Atherosclerosis shows preferential localization at sites where flow is either slow or disturbed and where WSS as well as its gradients are low [3]. The hypothesis that an increased plasma viscosity may be a link between cardiovascular risk factors and coronary atherosclerosis is supported by various studies [4]. According to non-Newtonian behavior, viscosity depends on the velocity gradient and varies along the course of the vessel. Henceforth, the variation depends on the applied flow conditions, the vascular geometry, and the flow particularities. However, little research has focused on the exact role of local viscosity differentiation within the coronary arterial tree in atherogenesis. This is due to the complex geometry, as well as to the small vessel diameters involved in the analysis.

In the early Computational Fluid Dynamics (CFD) works on the cardiovascular system, the blood was treated as a Newtonian fluid. In the last few years, treating the blood as a non-Newtonian fluid [10], a number of papers have been published dealing with the distribution of the: (a) WSS [3,5–8], (b) the molecular viscosity [9] and (c) the wall shear stress gradient (WSSG) [3] in the human coronary arteries.

The application of an appropriate non-Newtonian model for the cardiovascular flow analysis is crucial for achieving

* Corresponding author at: AHEPA University Hospital, Aristotle University of Thessaloniki, 1 St. Kyriakidi Street, 54636 Thessaloniki, Greece. Tel.: +30 2310994837; fax: +30 2310994837.
E-mail address: yan@med.auth.gr (G.D. Giannoglou).

1350-4533/$ – see front matter © 2007 IPEM. Published by Elsevier Ltd. All rights reserved.
doi:10.1016/j.medengphy.2007.02.001

acceptable results. Non-Newtonian flow comparison models in human right coronary arteries (RCA) were reported [11]. The magnitude of WSS as well as the local and global importance factors were analyzed for four different RCA vessels using five different non-Newtonian models. However, the tested arteries, did not encounter any bifurcation. Bifurcated regions of the left coronary artery (LCA) tree are of paramount importance, since the nearby and opposite to the flow divider areas, where low strain rates occur, are regions prone to atherosclerosis [3,6]. Adequate blood viscosity models are needed to capture the main flow characteristics at low strain rates [12]. It is in these regions that high gradients of strain rates also occur. Many non-Newtonian models exist, but none of them is universally accepted. In the current work, seven non-Newtonian models and a Newtonian one were compared in a real human LCA tree. These models included Newtonian, Carreau [2], Modified Cross Law (Carreau–Yasuda) [13], Power Law [14], non-Newtonian Power Law [14], Generalized Power Law [15], Casson [16], Walburn–Schneck Law [17].

Intravascular ultrasound (IVUS) allows transmural visualization of coronary arteries and direct measurements of lumen, plaque and vessel dimensions [18]. IVUS is an ideal tool for the assessment of the mechanisms that may be involved in the localization and progression of atherosclerosis. IVUS LCA tree data, from a particular patient, is used to construct the geometry. These data include the left main coronary artery (LMCA), the left anterior descending (LAD) and the left circumflex artery (LCxA). The tested vessel presents normal, non-stenotic, geometry throughout.

The aims of this research work include:

(1) To compare results derived by various non-Newtonian molecular viscosity models.
(2) To study the local non-Newtonian importance factors I_L using various non-Newtonian molecular viscosity models [11].
(3) To study the global non-Newtonian importance factors I_G using various non-Newtonian molecular viscosity models [11].
(4) To compare the WSS distribution using various non-Newtonian molecular viscosity models.
(5) To compare the WSSG under resting, normal and exercise flow conditions, using non-Newtonian molecular viscosity models.
(6) To guide the perspective cardiovascular engineering analyst, via CFD analysis, to realize the capabilities and limitations of molecular viscosity models.

To the best of our knowledge, there is no published computational work comparing the molecular viscosity, WSS and WSSG of 3D reconstructed geometrically correct LCA bifurcation using various non-Newtonian blood viscosity models.

2. Methods

2.1. Catheter path reconstruction

The applied reconstruction method has been described and validated in details elsewhere [19–21]. Briefly, the IVUS catheter was inserted through a 6F guiding catheter into the coronary artery. A biplane coronary angiogram was recorded having the catheter located at its most distal position. From each angiographic projection, a single end-diastolic frame was selected corresponding to the peak of R-wave on ECG. With a well-validated quantitative angiography software package (CAAS II, Pie Medical Imaging), the luminal outlines were semi-automatically detected in each frame. Both end-diastolic frames were then transferred into a commercially available software package (Rhinoceros 3.0, Seattle, WA, USA) in order to delineate the IVUS catheter from the tip of the transducer up to the outlet of the guiding catheter. To improve the detection accuracy, both images were rectified with simple contrast and brightness adjustments. The resultant 2D b-spline curves were vertically extracted to the corresponding angiographic planes and intersected creating a 3D curve that corresponded to the geometrically correct IVUS catheter path.

2.2. IVUS images acquisition and segmentation

The IVUS procedure was performed using a mechanical imaging system (ClearView, Boston Scientific, Natick, MA, USA) and a 2.6F sheath-based catheter, incorporating a 40 MHz single-element transducer rotating at 1800 rpm and yielding 30 fps (Atlantis SR Pro, Boston Scientific, Natick, MA, USA). A motorized pullback device was used to withdraw the catheter from its most distal position to the outlet of the guiding catheter at a constant speed of 0.5 mm/s. All ultrasound data was digitized by a frame-grabber and the end-diastolic images were selected. In the gated sequence of IVUS images, the lumen and media-adventitia borders were semi-automatically detected using a custom-developed computer algorithm based on active contour models, also known as snakes [20].

2.3. Generation of 3D lumen

Each couple of contours (luminal and media-adventitia) was assigned equidistantly at the 3D reconstructed catheter path. Since angular rotation of the IVUS catheter during pullback could distort the real geometry of the reconstructed artery, the correct rotational orientation of the luminal contours was determined by applying a Frenet–Serret theorem-based algorithm. Finally, the correctly orientated luminal contours were interpolated with additional intermediate contours, generating a 3D luminal volume. To determine the spatially correct orientation of the reconstructed vessel, the interpolated lumen was iteratively rotated searching for the best possible match with the corresponding angiographic luminal edges.

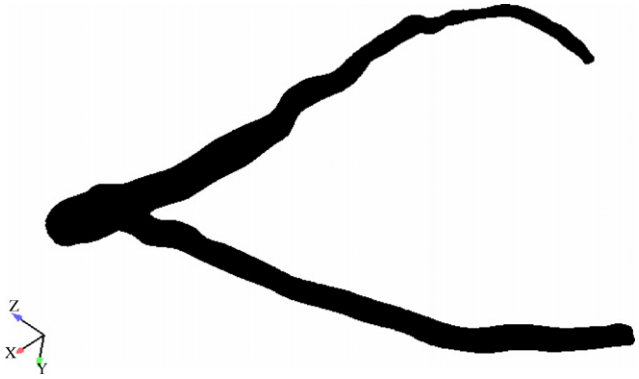

Fig. 1. Left coronary artery (LCA) geometry used for the computational analysis.

With the above approach the LCA and LCxA lumens were reconstructed separately and they manually merged according to their real geometrical configuration in humans.

2.4. Computational grid

All lumen geometrical data was transferred into a specialized pre-processing program for grid generation (Fluent Inc., Gambit, Lebanon, NH, USA). In total 134,715 grid nodes were utilized giving rise to a 466,001 computational tetrahedral. Fig. 1 shows details of the utilized non-structured grid of the human LCA tree. The grid in a typical proximal cross-section is shown in Fig. 2. The used mesh was based on the computational results of mesh-independence studies. Meshes were created with a larger number of nodes in the radial direction. Thus, the number of nodes located in the near to the artery wall areas was significantly higher to those at vessel wall centre-line regions. An alternative grid adaptation technique based on the WSS distribution was proved to be inadequate, since most of the grid nodes were located at the outlet regions of the vessel where the WSS values are high. The number of nodes used to define the mesh independence increased from 44,452 initially to 59,524 nodes and at a later stage to 134,715 nodes. The relative error in the derived hemodynamics parameter of WSS was calculated and used as a quantitative measure of the grid density effects upon the results.

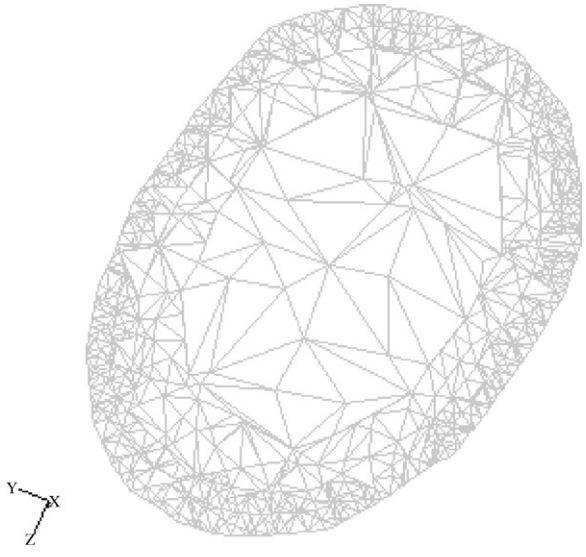

Fig. 2. Non-structured grid of the 3D human left coronary artery (LCA) used for computational analysis. Example of the grid in a typical proximal cross-section.

2.5. Flow equations, boundary flow conditions and CFD

The velocity was assumed to be uniform at the orifice of LMCA. The applied inflow conditions mimic typical coronary flow velocity under resting conditions (0.17 m/s), moderate flow (0.34 m/s) and exercise flow (0.68 m/s). Flow discharges were set analogous to the third power of the branching vessel diameter according to Murray's Law [22]. All computational grid data, as well as all physical flow data determined from the boundary conditions, were imported into the main CFD solver (Fluent Inc., Fluent 5.5, Lebanon, NH, USA) [23]. The numerical code solves the governing momenta equations. In general, these equations solve for mass, momentum and energy conservation. Flow is considered as three-dimensional, steady, laminar, with no external forces applied on it, while the arterial wall is comprised from non-elastic and impermeable material. The governing flow equations are given in Appendix A. The applied numerical code utilizes a segregated solver of implicit formulation. A standard discretization technique is applied for the pressure. The pressure–velocity coupling is based on the SIMPLEC technique. First order-upwind discretization is applied for the momentum and energy equations. For a typical satisfactory convergence solution, a total of 500 time steps were required. Convergence was achieved when all mass, velocity component and energy changes, from iteration to iteration, were less than 10^{-8}.

2.6. Calculated variables

Molecular viscosity μ (kg/m s) values were calculated throughout the entire LCA including the LMCA, the LAD and the LCxA. All molecular viscosity and WSS values are shown in filled contours coupled with iso-contour line form.

The *local non-Newtonian importance factor* I_L is defined [11] as:

$$I_L = \frac{\mu}{\mu_\infty} \tag{1}$$

where μ_∞ is 0.00345 (kg/m s) and represents the undisturbed value of the dynamic blood viscosity. The distribution of this factor over the LCA clearly shows the non-Newtonian flow patches.

The averaged *global non-Newtonian importance factor* I_G is defined [11,15] as:

$$I_G = \frac{1}{N} \frac{[\sum_{i=1}^{\text{total grid nodes}} (\mu - \mu_\infty)^2]^{1/2}}{\mu_\infty} \times 100 \tag{2}$$

where i is the grid node index and incorporates the cells on all LCA walls, N is the total grid nodes (=134,715). The importance factor I_G is evaluated at each node on the surface of the artery. μ_∞ takes the value 0.00345 kg/m s, which is the undisturbed value of the dynamic viscosity. The I_G expresses the relative difference from the Newtonian value in percentage terms of each value of molecular viscosity. Values of I_G greater than 0.25 indicate non-Newtonian flow behavior.

Wall shear stress (N/m^2). For incompressible fluids and for non-slip conditions applied at the arterial wall, the spatial WSS is calculated as,

$$\mathrm{WSS} = \tau_w = -\mu \frac{\partial u_t}{\partial n}\bigg|_{\mathrm{wall}} \tag{3}$$

where μ (kg/m s) is the dynamic viscosity, u_t (m/s) the tangential to the wall velocity and n is the unit vector perpendicular to the wall.

The *area averaged wall shear stress WSS* (N/m^2), is defined as:

$$\text{area averaged WSS} = \frac{1}{A_o} \sum_{i=1}^{\text{total cells}} |\mathrm{WSS}|_i a_i \tag{4}$$

where i is the cell index on all LCA walls, a_i the cell area and A_o is the total surface area (=10.865 cm^2) of the tested LCA. It is utilized to measure the degree of WSS variation along the surfaces of the LCA.

Wall shear stress gradient WSSG (N/m^3). The calculation of the local magnitude for the WSSG is defined [3],

$$\mathrm{WSSG} = \sqrt{\left(\frac{\partial \tau_w}{\partial x}\right)^2 + \left(\frac{\partial \tau_w}{\partial y}\right)^2 + \left(\frac{\partial \tau_w}{\partial z}\right)^2} \tag{5}$$

The components of the WSSG may have different effects upon endothelial cells. Most diagonal components generate intercellular tension while the off-diagonal components may contribute to intercellular shearing forces [24].

The severity parameter (SP, N/m^3) [25,26], is defined as,

$$\mathrm{SP} = \frac{1}{A_o} \sum_{i=1}^{\text{total cells}} |\mathrm{WSSG}|_i a_i \tag{6}$$

The SP is utilized to measure the degree of spatial variation of WSS along the surfaces of the LCA. High SP values denote high spatial flow variation.

2.7. Non-Newtonian molecular viscosity models

In total, seven different non-Newtonian molecular viscosity models – and one Newtonian model – are incorporated into the main CFD solver (Appendix B). The applied input parameters for each model are also shown. For comparison purposes, two graphs showing the strain rate versus molecular viscosity are presented. Fig. 3a shows the strain rate (s^{-1}) versus molecular viscosity (Pa s) for non-Newtonian Power Law and Fig. 3b shows the same distribution for the Generalized Power Law blood model. The two power laws exhibit different behavior.

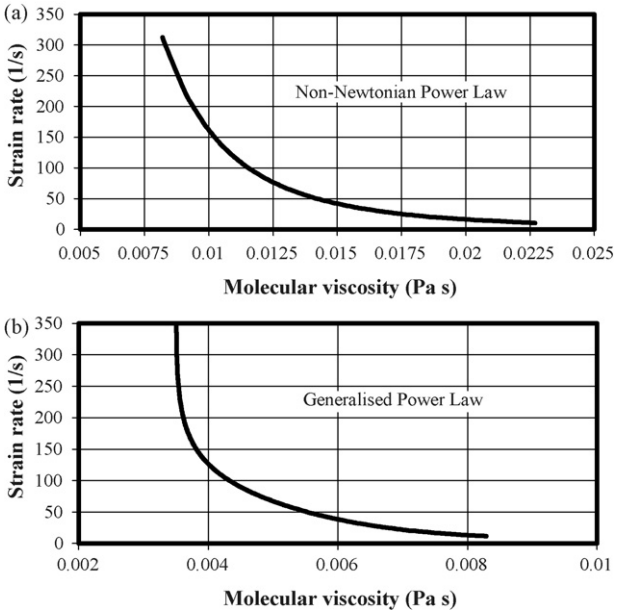

Fig. 3. Strain rate vs. molecular viscosity for: (a) non-Newtonian Power Law and (b) Generalized Power Law blood model.

The Generalized Power Law model is a wider form of non-Newtonian molecular viscosity behavior. At small strain rate values $\dot{\gamma}$ behaves as the Power law model. At very high-strain rates >300 (s^{-1}), the molecular viscosity value reaches 0.00345 (Pa s), which is the widely accepted value for Newtonian molecular viscosity of blood flow. It has the Casson Law model as a special case [15].

The Power Law and the non-Newtonian Power Law models use similar parameters. The constant factor for the Power Law is 0.035 and the power value n for the strain rate ($\dot{\gamma}$) is 0.6. The corresponding values for the non-Newtonian model values are 0.0526 and 0.7.

The Casson [16] as well as the Walburn–Schneck [17] Law models incorporate the hematocrit (volume red blood cells/volume whole blood). For the former the applied hematocrit value H is 37.0 and 40.0% for the later. Walburn–Schneck model is essentially another form of non-Newtonian Power Law model. At high-strain rates the Carreau model behaves as a Newtonian model. The Modified Cross model is a form of the Carreau–Yasuda model.

3. Results

3.1. Molecular viscosity

Fig. 4 shows the molecular viscosity (kg/m s) magnitude distribution at the main LCA bifurcation of the LCA tree using the Carreau Law, Modified Cross Law, Power Law, non-Newtonian Power Law, Generalized Power Law, Casson Law and Walburn–Schneck Law models, respectively. For the

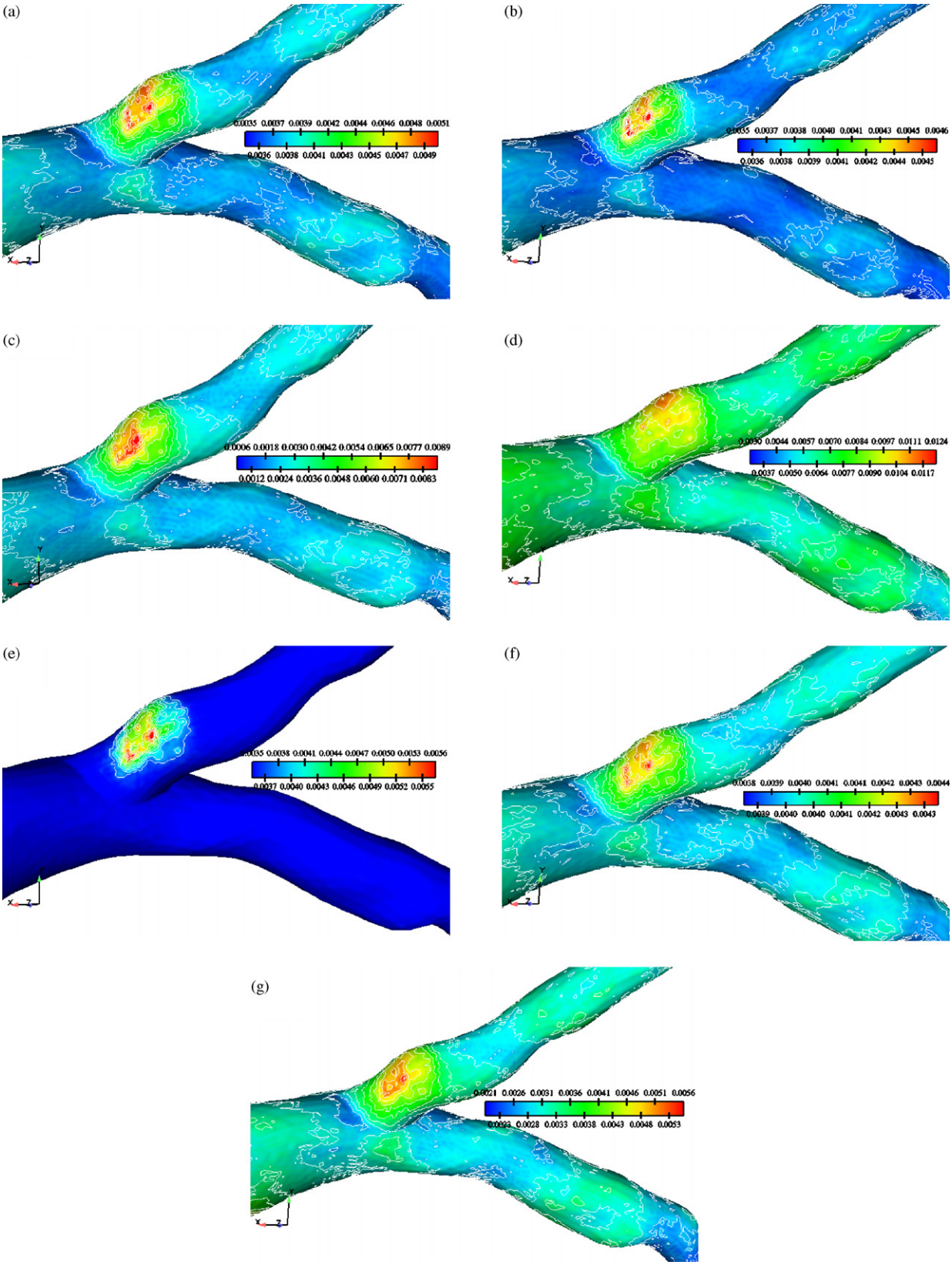

Fig. 4. Contour plots of the molecular viscosity (kg/m s) magnitude distribution. Contour labels range from 1 to 15 and correspond to 15 color levels shown in the bar. (a) Carreau Law model, (b) Modified Cross Law model, (c) Power Law model, (d) non-Newtonian Power Law model, (e) Generalized Power Law model, (f) Casson Law model, (g) Walburn–Schneck Law model. (For interpretation of the references to color in this figure legend, the reader is referred to the web version of the article.)

non-Newtonian Power Law model, the molecular viscosity values range from 0.0044 to 0.0114 kg/m s, see Fig. 4d. Note that the above range is the widest one of all tested molecular viscosity models. The range between maximum and minimum molecular viscosity values using Carreau Law (Fig. 4a), Modified Cross Law (Fig. 4b), Generalized Power Law model (Fig. 4e), and Casson Law (Fig. 4f), for the same LCA bifurcation region, is relatively narrow (0.00345–0.0065 kg/m s). Even narrower is the range of molecular viscosity values for the Walburn–Schneck Law model (0.0024–0.0055 kg/m s), Fig. 4g. The Power Law (Fig. 4c) model gives molecular values ranging between 0.0006 and 0.0093 kg/m s.

3.2. Non-Newtonian local importance factor I_L

Factor $I_{L,}$ defined in Eq. (1), expresses the degree of molecular viscosity deviation from Newtonian behavior. Fig. 5 shows the contours of factor I_L for the non-Newtonian Power Law model. The normalization is performed against the Newtonian molecular viscosity value (=0.00345 kg/m s). The I_L factor attains values greater than 1.0 throughout the LCA. For the bifurcation, shown in Fig. 5, this value reaches 3.69 units. Patches of highly non-Newtonian behavior are located in the concave region of the LCA bifurcation, opposite the flow divider. Note that the enlarged concave configuration characterizes the LMCA vessel of the tested patient.

3.3. Non-Newtonian global importance factor I_G

For a particular LCA artery geometry and a particular inlet flow condition, there is a distinct global importance factor I_G, defined in Eq. (2). In turn the application of various molecular viscosity models yield different I_G values for the same artery and inlet flow condition. Tables 1–3 show the factor I_G using various molecular viscosity models at the averaged inlet flow velocity magnitude of 0.17, 0.34 and 0.68 m/s, respectively. In general, as the inlet velocity value increases, the I_G value tends to decrease. Low values of I_G (<0.25) indicate that the blood behaves as Newtonian fluid. For all applied inlet flow velocities, it is the Non-Newtonian Power Law model that yields values of I_G greater than 0.25.

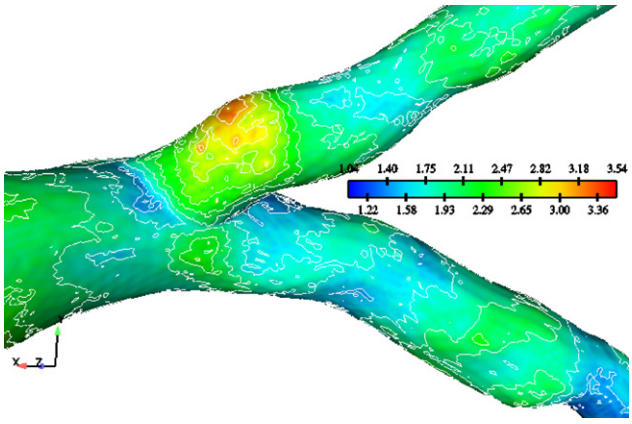

Fig. 5. Contours of local non-Newtonian importance factor I_L. The I_L factor refers to non-Newtonian Power Law molecular viscosity ratio. Non-dimensionalization is performed against Newtonian molecular viscosity value (=0.00345 kg/m s).

3.4. Wall shear stress

The WSS distribution focuses in the LCA bifurcation region. From the hemodynamic point of view this area is the most important LCA region. Fig. 6 presents eight plots of the WSS iso-contour distribution at the LCA bifurcation; each plot corresponds to a different molecular viscosity model. Thus, a comparison of the WSS distribution between the various viscosity models can be easily made. All plots indicate that at regions opposite to the flow divider, dominant low WSS values occur. Note that the WSS values increase from proximal to distal LAD parts.

This WSS pattern is predicted in all molecular viscosity models. However, each model has its own particular distribution. For the non-Newtonian Power Law model, the WSS values range from 0.78 to 12.48 N/m^2, in the region opposite to the flow divider, Fig. 6e. The WSS contours of the entire LCA tree are shown in Fig. 7. The WSS values, for the Newtonian model in the bifurcation region, range

Table 1
Global non-Newtonian importance factor I_G using various models at averaged inlet velocity magnitude of 0.17 m/s (rest)

	Walburn–Schneck	Non-Newtonian Power Law	Generalized Power Law	Power Law	Carreau	Casson	Modified Cross
I_G	0.161	0.767	0.061	0.120	0.104	0.118	0.067

Table 2
Global non-Newtonian importance factor I_G using various models at averaged inlet velocity magnitude of 0.34 m/s (normal)

	Walburn–Schneck	Non-Newtonian Power Law	Generalized Power Law	Power Law	Carreau	Casson	Modified Cross
I_G	0.208	0.562	0.029	0.145	0.073	0.107	0.181

Table 3
Global non-Newtonian importance factor I_G using various models at averaged inlet velocity magnitude of 0.68 m/s (exercise)

	Walburn–Schneck	Non-Newtonian Power Law	Generalized Power Law	Power Law	Carreau	Casson	Modified Cross
I_G	0.249	0.431	0.015	0.164	0.050	0.100	0.033

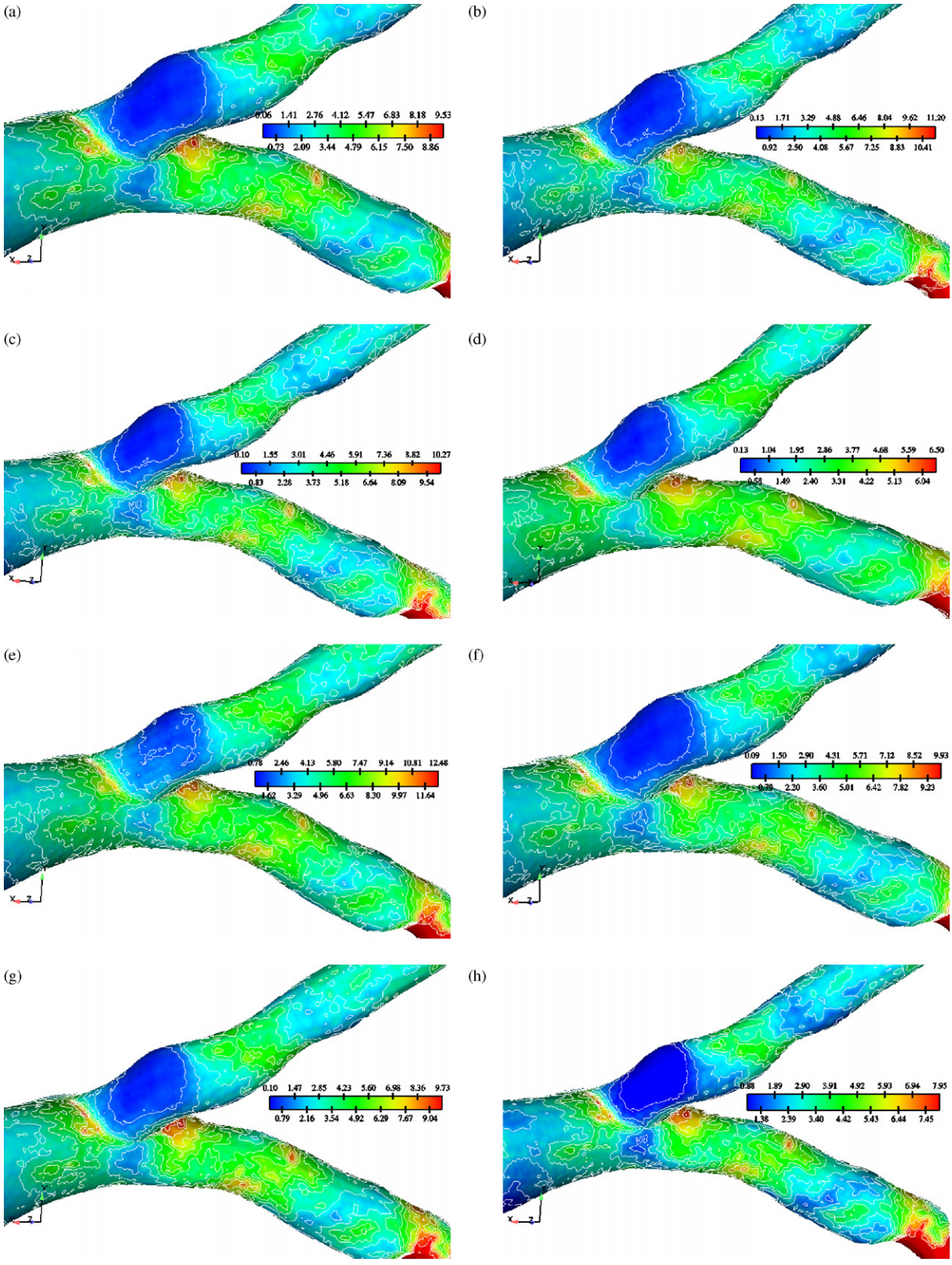

Fig. 6. Contour plots of the wall shear stress (WSS, N/m^2) magnitude distribution. Contour labels range from 1 to 15 and correspond to 15 color levels shown in the bar. (a) Newtonian Law model, (b) Carreau Law model, (c) Modified Cross Law model, (d) Power Law model, (e) Non-Newtonian Power Law model, (f) Generalized Power Law model, (g) Casson Law model, (h) Walburn–Schneck Law model. (For interpretation of the references to color in this figure legend, the reader is referred to the web version of the article.)

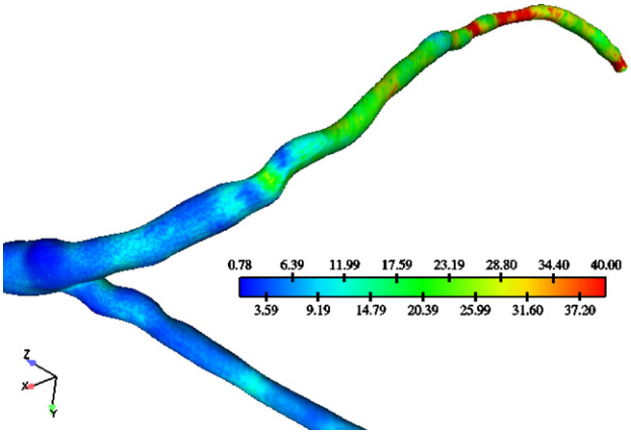

Fig. 7. Contour plots of the wall shear stress (WSS, N/m^2) magnitude distribution of the 3D reconstructed human left coronary artery (LCA) using the non-Newtonian Power Law molecular viscosity model. Details of the bifurcation region are shown in Fig. 6e.

from 0.06 to 9.53 N/m^2 (Fig. 6a). For all other models, the WSS values range from 0.1 to 10.0 N/m^2. Area averaged wall shear stress (WSS, N/m^2) values are calculated using Eqs. (3) and (4). Table 4 shows the calculated area averaged WSS values, using various molecular viscosity models. The non-Newtonian Power Law model averaged WSS value is 13.34 N/m^2. The Power Law model gives the smaller area averaged wall shear stress value of 5.82 N/m^2.

3.5. Wall shear stress gradient

Any non-zero value of the WSSG, calculated using Eq. (5), denotes a non-uniform hemodynamic environment. At the LMCA bifurcation region, high WSSG values tend to form a "ring" located at the origin of the LCxA (not shown). Further observation reveals that the distribution of WSSG is highly non-uniform. WSSG values increase in the downstream flow. The severity parameter values (SP, N/m^3) are calculated using Eq. (6). Table 5 shows the calculated SP values using various molecular viscosity models at 0.17 m/s inlet flow velocity. The non-Newtonian Power Law model calculated SP value is 7038.6 N/m^3. The lowest SP value is 2346.6 and it is derived using the Power Law viscosity model. All other viscosity models give SP values in the order of 8800.0 N/m^3. It is apparent that the differences in the calculated SP values, using different molecular viscosity models, are great. This is due to the high sensitivity of the SP parameter. Higher inlet flow velocities give higher SP values (not shown).

4. Discussion

Plasma viscosity distribution within the coronary artery tree may represent a risk factor for atherosclerosis [27]. In particular [28], hypertension, hyperlipidemia and diabetes increase whole blood viscosity. It is known that, in order to maintain normal flow within the arterial system, the blood viscosity and the erythrocyte deformability should be adequately adapted to flow conditions [1]. For atherosclerotic coronary vessels, the effect of non-Newtonian viscosity on hemodynamics can be more complicated than in a non-diseased vessel [2]. Reduced erythrocyte deformability is of vital importance in arterial stenosed areas, resulting in an increase in both local strain rate and whole blood viscosity. Moreover, increased viscosity in an area of plaque rupture could have a prothrombotic effect [1]. It is known [6] that there is a significant relation between high molecular viscosity and atherosclerosis (vessel wall thickening) in human coronary arteries. Long residence time in endothelium results in increased lipoprotein uptake leading to the thickening of the arterial vessel wall [6]. The role of viscosity in the development and progression of cardiac disease is very important. Henceforth, the selection and application of an appropriate viscosity model for CFD analysis is crucial for achieving acceptable results. The main goal of this work was to assess the difference between Newtonian and non-Newtonian viscosity models of blood flow in a human LCA tree.

Our results, using any of the molecular viscosity models, show that there are three distinct regions within the flow possessing high molecular viscosity: (1) the region located near the center of the cross-sectional area of any segment, which is characterized by high velocity magnitude and occupies a large section of the lumen, followed by a region of reduced molecular viscosity values extending up to the endothelium; (2) the proximal LCA regions where the magnitude of molecular viscosity decreases from proximally to distally of the flow divider Fig. 4f and g. This is due to the fact that the vessel geometry is highly tapered. Thus, the flow velocity increases from proximal to distal parts. Subsequently, the WSS increases and the molecular viscosity decreases.) (3)

Table 4
Area averaged wall shear stress (WSS, N/m^2) using various molecular viscosity models

Walburn–Schneck	Newtonian	Non-Newtonian Power Law	Generalized Power Law	Power Law	Carreau	Casson	Modified Cross
8.84	11.92	13.34	12.04	5.82	12.28	12.89	12.18

Table 5
Area averaged wall shear stress gradient (WSSG, N/m^3) (SP parameter) using various molecular viscosity models

Walburn–Schneck	Newtonian	Non-Newtonian Power Law	Generalized Power Law	Power Law	Carreau	Casson	Modified Cross
5024.9	8713.8	7038.6	8803.4	2346.6	8786.0	9392.5	8800.7

The lateral walls opposite to the flow divider (Figs. 4a–g and 7). The tested LCA exhibits a relatively large concave region opposite to the flow divider, where low blood viscosity occurs (Fig. 5). Also, the lateral walls of bifurcation, opposite flow divider, are characterized by low WSS and low velocity values. However, the preserved molecular viscosity at low level values as well as the erythrocyte deformability usually constitute physiologic adjustments in humans to maintain normal flow in the coronary arteries. In all complex patterns of molecular viscosity distribution, using any of the non-Newtonian blood flow models, the endothelial regions in the opposite to flow divider at the outer walls of the major bifurcation attain high values (Fig. 4a–g). Low strain rates appear in these regions and the capabilities of the various blood models are clearly seen in the above figures. At high-strain rates, the differences in molecular viscosity values between Newtonian and non-Newtonian blood flow models are small. Nearly all blood flow models, except Walburn–Schneck and Power Law, have as a lower blood viscosity limit the value of the Newtonian blood flow viscosity (=0.00345 Pa s). The above is true for all applied blood flow models and partially true for the non-Newtonian Power Law blood flow model (Fig. 4d). The global non-Newtonian importance factor I_G, using various blood viscosity models, does not decrease monotonically with increasing inlet velocity magnitude [11] (Tables 1–3). The non-Newtonian Power Law, Generalized Power Law, Carreau and Casson models decrease the I_G value with increasing inlet velocity. In the opposite direction are the Walburn–Schneck, Power Law and Modified Cross models, which do not sufficiently describe the blood flow characteristics. However, all models except the non-Newtonian Power Law one give I_G values less than 0.25, which assumes to be the limit for Newtonian flow behavior.

In simulating Newtonian fluids, the re-circulation zone extends almost into the central cross-section of the vessel. However, a non-Newtonian behavior in low shear regions minimizes the extent of re-circulation zones [29]. These zones usually appear along a certain [11] distance close to the arterial wall. Researchers [11] suggest the use of the Generalized Power Law model, Appendix B, at low shear rates, in order to achieve satisfactory WSS approximation. Their proposal [11] comes from simulating four different RCA segments using five viscosity models at different Reynolds numbers ranging from 20 to 1000. For the tested LCA tree and particular inlet flow velocity, the WSS distribution yields a consistent pattern for all non-Newtonian models (Fig. 6b–h). The WSS pattern is similar even for the Newtonian model (Fig. 6a). In case of LMCA bifurcation, low WSS values tend to form a "ring" located at the origin of the LCxA (Fig. 6a–h). This region, particularly the one included in the concave part, exhibits very low WSS values and is thus susceptible to development of atherosclerosis. The WSS patterns differ most significantly where the strain rate is low. The Newtonian blood flow treatment is considered to be a good approximation at mid and high-strain rates. The area averaged WSS value for the entire LCA tree using the Newtonian model is 11.92 N/m^2. This value is close to the WSS values ($\sim$12.0 N/m^2) derived using the non-Newtonian Power Law, the Generalized Power Law, the Carreau, the Casson and the Modified Cross blood viscosity models. The Walburn–Schneck and the Power Law models give 8.84 and 5.82 N/m^2, which are considered to be low. Equally unaccepted results are derived with the area averaged wall shear stress gradient (or the SP parameter) using Walburn–Schneck and the Power Law models. The SP parameter is highly sensitive and it is a better hemodynamic factor to assess the WSS behavior using various viscosity models.

4.1. Limitations

In the current study the inlet blood flow velocity was assumed to be constant. Indisputably, the inlet flow velocity profile affects the flow analysis, particularly in regions close to the inlet. Numerical experimentation was previously carried out [6] for 2D analysis, with regard to the shape of the inlet velocity profile using a plug velocity profile as well as a blunt velocity profile. The results (just downstream form the inlet) showed good correlation ($p < 0.01$) as those using a parabolic profile. It is the magnitude of physical parameters, which is mostly affected by the inlet profile, rather than the pattern of their distribution.

The time-dependent nature of the blood flow field further complicates the problem. The current analysis assumed that the flow was steady. This limits the real behavior and the derived results are representative only to the averaged flow behavior. Despite all this, the current results are not far away from those of pulsatile flow since it has been proved [5,30] that averaged unsteady flow results are similar to the ones derived from steady flow.

The arterial vessel walls have been assumed to be impermeable, smooth and inelastic, although it is known that real arterial walls present irregularities and because of the elastic nature of these boundaries the geometry alters during the cardiac cycle. Furthermore, in our calculations we did not take into account the coronary artery movement during the cardiac cycle. However, coronary artery movement, up to 1 Hz frequency, only slightly affects the velocity changes (maximum 6%) [31]. Therefore, our results are not significantly influenced by this assumption.

5. Conclusions

In this study the usefulness and limitations of different molecular viscosity models are compared using resting, normal and exercise flow conditions in an IVUS derived LCA tree. Results indicate that patches of highly non-Newtonian behavior are located in the concave region of the LCA bifurcation, opposite to the flow divider. Calculated area averaged wall shear stress values using various molecular viscosity models are 12.0 N/m^2, while area averaged wall shear stress

gradient values are approximately 8800.0 N/m^3. The WSS distribution yields a consistent LCA tree pattern for nearly all non-Newtonian models. High molecular viscosity and low wall shear stress and wall shear stress gradient values appear at proximal LCA regions at the outer walls of the major bifurcation. The capabilities of the various non-Newtonian blood models are clearly elucidated. The non-Newtonian Power Law, Generalized Power Law, Carreau and Casson and Modified Cross blood viscosity models give comparable molecular viscosity, WSS and WSSG values. The Power Law and Walburn–Schneck models overestimate the non-Newtonian global importance factor I_G and underestimate the area averaged WSS and WSSG values. The Newtonian blood flow treatment is considered to be a good approximation at mid and high-strain rates. In general, the non-Newtonian Power Law and the Generalized Power low blood viscosity models are considered to approximate the molecular viscosity and WSS calculations in a more satisfactory way.

Acknowledgement

The authors thank Dr. Nikolaos Tsiampas for his help in the editing of the manuscript.

Conflict of interest

None.

Appendix A. Flow equations

The governing flow equations are:

$$\frac{\partial \rho}{\partial t} + \frac{\partial}{\partial x_i}(\rho u_i) = S_m$$

where ρ (kg/m^3) is the density, t (s) the time, u_i (m/s) the velocity components along the x_i, (m) axes and S_m is the added or subtracted mass of fluid in the flow field. The conservation of momentum along the i direction is written,

$$\frac{\partial}{\partial t}(\rho u_i) + \frac{\partial}{\partial x_j}(\rho u_i u_j) = -\frac{\partial p}{\partial x_i} + \frac{\partial \tau_{ij}}{\partial x_j} + \rho g_i + F_i$$

Here, p (N/m^2) is the static pressure, τ_{ij} (N/m^2) the shear stress tensor, ρg_i (N/m^3) and F_i (N/m^3) are gravity and externally acting forces, respectively.

Appendix B. Newtonian and Non-Newtonian models

Seven non-Newtonian and one Newtonian computational analyses are performed using the following blood viscosity models:

1. Newtonian model
   $\mu = 0.00345$ Pa s
2. Carreau model [6]
   $$\mu = \mu_\infty + (\mu_0 - \mu_\infty)[1 + (\lambda\dot\gamma)^2]^{(n-1)/2}$$
   where $\lambda = 3.313$ s, $n = 0.3568$, $\mu_0 = 0.056$ Pa s, $\mu_\infty = 0.00345$ Pa s, and $\dot\gamma$ is the strain rate.
3. Modified Cross Law model (Carreau–Yasuda model) [29]
   $$\mu = \mu_\infty + \frac{\mu_0 - \mu_\infty}{[1 + (\lambda\dot\gamma)^b]^a}$$
   where $\mu_0 = 0.16$ Pa s, $\mu_\infty = 0.0035$ Pa s, $\lambda = 8.2$ s, $a = 1.23$, and $b = 0.64$.
4. Power Law model [2]
   $$\mu = \mu_0(\dot\gamma)^{n-1}$$
   where $\mu_0 = 0.035$ and $n = 0.6$.
5. Non-Newtonian Power Law model [14]
   According to this law, the fluid shear stress, denoted by τ (N/m^2), is calculated as,
   $$\tau = [\eta(\dot S)]\dot S, \quad \eta(\dot S) = k e^{T_0/T}\dot S^{n-1}, \quad \dot S = \frac{\partial u_i}{\partial x_j} + \frac{\partial u_j}{\partial x_i}$$
   where k = consistency index (kg s^{n-2}/m), n = power-law index, T_0 = reference temperature (K), μ_0 = minimum viscosity limit (kg/m s), μ_∞ = maximum viscosity limit (kg/m s). The actual values are: $\mu_0 = 0.0001$ Pa s, $\mu_\infty = 0.1$ Pa s, $n = 0.7$, $T_0 = 310$ K, $k = 0.01691$ kg s^{n-2}/m.
6. Generalized Power Law model [15]
   $$\mu = \lambda|\dot\gamma|^{n-1} \quad \text{(units in poise : 1.0 P = 0.1 Pa s)}$$
   where
   $$\lambda(\dot\gamma) = \mu_\infty + \Delta\mu \exp\left[-\left(1 + \frac{|\dot\gamma|}{\alpha}\right)\exp\left(\frac{-b}{|\dot\gamma|}\right)\right] \text{ and}$$
   $$n(\dot\gamma) = n_\infty - \Delta n \exp\left[-\left(1 + \frac{|\dot\gamma|}{c}\right)\exp\left(\frac{-d}{|\dot\gamma|}\right)\right]$$
   with $\mu_\infty = 0.035$, $n_\infty = 1.0$, $\Delta\mu = 0.25$, $\Delta n = 0.45$, $a = 50$, $b = 3$, $c = 50$ and $d = 4$.
7. Casson model [16]
   $$\mu = [(\eta^2 J_2)^{1/4} + 2^{-1/2}\tau_y^{1/2}]^2 J_2^{-1/2}$$
   where $|\dot\gamma| = 2\sqrt{J_2}$, $\tau_y = 0.1(0.625H)^3$ and $\eta = \eta_0(1 - H)^{-2.5}$ with $\eta_0 = 0.0012$ Pa s and $H = 0.37$.
8. Walburn–Schneck Law model [17]
   $$\mu = C_1 e^{HC_2}[e^{C_4(\mathrm{TPMA})/H^2)}](\dot\gamma)^{-C_3 H} \quad \text{(units in poise)}$$
   where $C_1 = 0.00797$, $C_2 = 0.0608$, $C_3 = 0.00499$, $C_4 = 14.585$ l/g, $H = 40$ and TPMA = 25.9 g/l.

References

[1] Becker RC. The role of blood viscosity in the development and progression of coronary artery disease. Cleve Clin J Med 1993;60:353–8.

[2] Cho YI, Kensey KR. Effects of the non-Newtonian viscosity of blood on flows in a diseased arterial vessel. Part 1. Steady flows. Biorheology 1991;28:241–62.
[3] Farmakis TM TM, Soulis JV, Giannoglou GD, Zioupos GJ, Louridas GE. Wall shear stress gradient topography in the normal left coronary arterial tree: possible implications for atherogenesis. Curr Med Res Opin 2004;20:587–96.
[4] Junker R, Heinrich J, Ulbrich H, Schonfeld R, Kohler E, Assman G G. Relationship between plasma viscosity and the severity of coronary heart disease. Arterioscler Thromb Vasc Biol 1998;18:870– 5.
[5] Soulis JV, Giannoglou GD, Chatzizisis YS, Farmakis TM, Giannakoulas GA, Parcharidis GE, et al. Spatial and phasic oscillation of non-Newtonian wall shear stress in human left coronary artery bifurcation: an insight to atherogenesis. Coron Artery Dis 2006;17(4):351–8.
[6] Giannoglou GD, Soulis JV, Farmakis TM, Farmakis DM, Louridas GE. Haemodynamic factors and the important role of local low static pressure in coronary wall thickening. Int J Cardiol 2002;86:27–40.
[7] Gibson CM, Diaz L, Kandarpa K, Sacks FM, Pasternack RC, Sandor T, et al. Relation of vessel wall shear stress to atherosclerosis progression in human coronary arteries. Arterioscler Thromb 1993;13(2):310–5.
[8] Krams R, Wentzel JJ, Oomen JA, Vinke R, Schuubiers JC, de Feyter PJ, et al. Evaluation of endothelial shear stress and 3D geometry as factors determining the development of atherosclerosis and remodeling in human coronary arteries in vivo. Combining 3D reconstruction from angiography and IVUS (ANGUS) with computational fluid dynamics. Arterioscler Thromb Vasc Biol 1997;17(10):2061–5.
[9] Soulis JV, Farmakis TM, Giannoglou GD, Hatzizisis IS, Giannakoulas GA, Parcharidis GE, et al. Molecular viscosity in the normal left coronary arterial tree. Is it related to atherosclerosis? Angiology 2006;57(1):33–40.
[10] Giannoglou GD, Soulis JV, Farmakis TM, Giannakoulas GA, Parcharidis GE, Louridas GE. Wall pressure gradient in normal left coronary artery tree. Med Eng Phys 2005;27(6):455–64.
[11] Johnston BM, Johnston PR, Corney S. Non-Newtonian blood flow in human right coronary arteries: steady state simulations. J Biomech 2004;37:709–20.
[12] Ghista DN, Van Vollenhoven E, Yang W-J, Reul H. Blood: rheology, hemolysis, gas and surface interactions. New York: S. Karger; 1979, 165 pp.
[13] Abraham F, Behr M, Heinkenschloss M. Shape optimization in unsteady blood flow: a numerical study of non-Newtonian effects. Comput Methods Biomech Biomed Eng 2005;8(3):201–12.
[14] Sharma K, Bhat SV. Non-Newtonian rheology of leukemic blood and plasma: are n and k parameters of power Law model diagnostic? Physiol Chem Phys Med NMR 1992;24:307–12.
[15] Ballyk PD, Steinman DA, Ethier CR. Simulation of non-Newtonian blood flow in an end-to-side anastomosis. Biorheology 1994;31:565–86.
[16] Fung YC. Biomechanics: mechanical properties of living tissues. 2nd ed. Berlin: Springer; 1993, 571 pp.
[17] Walburn FJ, Schneck DJ. A constitutive equation for whole human blood. Biorheology 1976;13(3):201–10.
[18] von Birgelen C, Klinkhart W, Mintz GS, Papatheodorou A, Herrmann J, Baumgart D, et al. Plaque distribution and vascular remodeling of ruptured and nonruptured coronary plaques in the same vessel: an intravascular ultrasound study in vivo. J Am Coll Cardiol 2001;37(7):1864–70.
[19] Coskun AU, Yeghiazarians Y, Kinlay S, Clark ME, Ilegbusi OJ, Wahle O, et al. Reproducibility of coronary lumen, plaque, and vessel wall reconstruction and of endothelial shear stress measurements in vivo in humans. Catheter Cardiovasc Interv 2003;60:67–78.
[20] Giannoglou GD, Chatzizisis YS, Sianos G, Tsikaderis D, Matakos A, Koutkias V, et al. In vivo validation of spatially correct three-dimensional reconstruction of human coronary arteries by integrating intravascular ultrasound and biplane angiography. Coron Artery Dis 2006;17(6):545–51.
[21] Chatzizisis YS, Giannoglou GD, Matakos A, Basdekidou C, Sianos G, Panagiotou A, et al. In-vivo accuracy of geometrically correct three-dimensional reconstruction of human coronary arteries: is it influenced by certain parameters? Coron Artery Dis 2006;17(6):545–51.
[22] Murray CD. The physiological principle of minimum work. I. The vascular system and the cost of blood volume. Proc Natl Acad Sci 1926;12:207–14.
[23] Kelkar KM, Patankar SV. Development of generalized block correction procedures for the solution of discretized Navier–Stokes equations. Lebanon, NH: Creare Inc.; 1988 [TM-459].
[24] Lei M, Giddens DP, Jones SA, Loth F, Bassiouny H. Pulsatile flow in an end-to-side vascular graft model: comparison of computations with experimental data. J Biomech Eng 2001;123:80–7.
[25] Kleinstreuer C, Lei M, Archie Jr JP. Flow input waveform effects on the temporal and spatial wall shear stress gradients in a femoral graft-artery connector. J Biomech Eng 1996;118(4):506–10.
[26] Kute SM, Vorp DA. The effect of proximal artery flow on the hemodynamicss at the distal anastomosis of a vascular bypass graft: computational study. J Biomech Eng 2001;123(3):277–83.
[27] Lowe GD, Drummond MM, Lorimer AR, Hutton I, Forbes CD, Prentice CR, et al. Relation between extent of coronary artery disease and blood viscosity. Br Med J 1980;280:673–4.
[28] Kensey KR, Cho YI, Chang M M. Effects of whole blood viscosity on atherogenesis. J Invasive Cardiol 1997;9:17–24.
[29] Liepsch D. An introduction to biofluid mechanics-basic models and applications. J Biomech 2002;35:415–43.
[30] Ku DN, Giddens DP, Zarins CK, Glagov S. Pulsatile flow and atherosclerosis in the human carotid bifurcation. Positive correlation between plaque location and low oscillating shear stress. Arteriosclerosis 1985;5(May–June (3)):293–302.
[31] Santamarina A, Weydahl E, Siegel Jr JM, Moore Jr JE. Computational analysis of flow in a curved tube model of the coronary arteries: effects of time-varying curvature. Ann Biomed Eng 1998;26(November–December (6)):944–54.